Cellular Oncology (2025) 48:815–834
https://doi.org/10.1007/s13402-025-01053-w

RESEARCH

High extracellular matrix stiffness upregulates TNNT1 to awaken dormant tumor cells in liver metastatic niches of gastric cancer

Linhua Ji[1] · Jie Peng[1] · Yuxuan Lin[1] · Yiqing Zhong[1] · Bo Ni[1] · Chunchao Zhu[1] · Zizhen Zhang[1]

Received: 30 October 2024 / Accepted: 4 March 2025 / Published online: 6 May 2025

Abstract

Background Liver is one of the target organs bearing the most frequent distant metastasis of gastric cancer (GC), and patients with GC liver metastasis suffering from poor prognosis. According to "seed and soil" theory, important and complex interactions between disseminated tumor cells (DTCs) and metastasis tumor microenvironment (MTM) have played a vital role in waking the dormant DTCs and promoting their proliferation. We have discovered that the aberrantly activated cancer associated fibroblasts (CAFs) could significantly increase the enrichment and stiffness of extracellular matrix (ECM). ECM with high stiffness could facilitate the accumulation of Troponin T1, slow skeletal type (*TNNT1*) in cytoplasm for dormant DTCs awaking and proliferation.

Methods We set off from observing the stiffness of ECM around liver metastatic niches of GC and performed in vivo and in vitro study for further study. Based on the gained information, we plan to further unveil the underlying mechanism and explore the clinical transformation value using the ex-vivo and patient derived xenograft (PDX) model.

Conclusion Our study aims to illustrate the relationship between ECM stiffness and tumor dormancy awakening in liver metastasis of GC and provide reliable theoretical and research basis for treatment of GC liver metastasis.

Keywords Gastric cancer · Liver metastasis · Extracellular matrix · Matrix stiffness · Tumor dormancy · TNNT1

1 Introduction

Gastric cancer (GC) is one of the most common and deadly malignant tumors in the digestive system worldwide, characterized by insidious onset, rapid progression, high propensity for metastasis, and elevated mortality rates [1, 2]. GC ranks second and third in terms of incidence and mortality among all malignancies, posing a significant threat to the health of people. Advanced GC exhibits highly invasive biological features and a predilection for distant metastasis, being a primary factor contributing to poor prognosis [1]. Liver metastasis is the most common form of distant organ metastasis in GC, with an incidence rate as high as 44% in late-stage patients, and a five-year survival rate below 10% in individuals [3, 4]. Therefore, investigating the mechanisms underlying GC liver metastasis and exploring clinical treatment strategies hold paramount scientific significance.

Based on the "seed and soil" theory, the outgrowth or metastasis is not solely determined by the characteristics of tumor cells themselves but is significantly influenced by tumor microenvironment (TME) [5]. In the context of disseminated tumor cells (DTCs), the metastasis tumor microenvironment (MTM) at target organs crucially determines their survival, implantation and outgrowth. Before the formation of MTMs, DTCs will face an alien microenvironment such as local cell rejection, chemically distinct environments from the primary tumor, and attacks by immune cells, leading to the elimination of most DTCs [6, 7]. The surviving DTCs may enter a state of dormancy, characterized by halted cell cycles, reduced expression of most genes, minimal material exchange with the microenvironment, and resistance to external stimuli [8, 9]. Dormant tumor cells are difficult to detect yet exhibit strong resistance to treatment [10]. DTCs at

Linhua Ji, Jie Peng and Yuxuan Lin contributed equally to this work.

✉ Jie Peng
peng-jie@sjtu.edu.cn

✉ Bo Ni
nibo9465@163.com

✉ Chunchao Zhu
zhuchunchao@renji.com

✉ Zizhen Zhang
zzzhang16@hotmail.com

[1] Department of Gastrointestinal Surgery, Ren Ji Hospital, School of Medicine, Shanghai Jiao Tong University, Shanghai, People's Republic of China

dormant phase remain quiescent in target organ, awaiting formation of suitable MTMs to awaken and achieve metastatic niches establishment. This dormancy-awakening mechanism serves as a survival strategy for DTCs, enhancing their resilience by allowing them to remain in a prolonged "standby" state within the target organ and resume growth when conditions are favorable [8, 9, 11]. The mechanisms underlying the awakening of dormant tumor cells remain poorly understood but are closely associated with tumor metastasis, recurrence, and drug resistance. Therefore, a system to explore and trace dormancy-awakening is important. Leveraging a cell model reported in 2014, we set off to explore [12]. Dormant cells will remain at G0 phase of the cell cycle characterized by halted cell division and during which, cyclin-dependent kinase (CDK) complex inhibitor p27 will be expressed to hamper CDK activity, maintaining cells in a dormant state; while upon entry into the G1 phase, p27 undergoes degradation, causing its disappearance [13]. In the dormant-awakening cell model, p27 protein is fused with green fluorescent protein (GFP) and artificially engineered a mutation resulting in lacking binding affinity against CDK ($p27K^{-}$). The GFP-$p27K^{-}$ expressed cells can enter G1 phase without hindrance, accompanied by degradation of which and disappearance of green fluorescence, thereby making it possible for observation of dormancy-awakening progression. We also marked cells with mCherry, thus cells exhibiting red & green fluorescence were recognized to remain in a dormant state, while ones displayed only red fluorescence were classified to be activated. Through the combined use of this cell model and the intrasplenic injection liver metastasis mouse model, we simulated the dormant-awakening process of tumor cells in vivo and filtered out key genes involved.

Increasing research has correlated local tissue stiffness with various diseases, particularly in cancers [14, 15]. Alterations in tissue stiffness significantly affect cellular biological behaviors and functions of tumor cells. The influence of extracellular matrix (ECM) stiffness on cellular behavior may relate to the physical pressures exerted on cells [15, 16]. Within tumors, cells situated in the complex TME are notably sensitive to changes in ECM stiffness and the resultant mechanical pressures [17]. Around metastatic niches, the primary determinants of TME tissue stiffness include the density and structure of nearby ECM cells and their related secreted proteins. Among them, cancer-associated fibroblasts (CAFs) are the predominant stromal cell type influenced by TME, exhibiting enhanced nutritional functions; while recent studies have highlighted the supportive role of CAFs in regulating stiffness of TME [18, 19]. The essential components of ECM, secreted by stromal cells, include a variety of molecules such as proteoglycans, matricellular proteins, and fibronectins, with collagen I and II (COL-I & II) being most significant. Notably, reports have also suggested that lysyl oxidase (LOX), originating mainly from CAFs, is among the crucial molecules determining ECM stiffness via mediating covalent bonding of adjacent collagen molecules or intra-molecular bonding within collagen molecules together with TGM2 to increase ECM stiffness, thereby promoting tumor progression [20–22]. Inspired by these findings, we conducted tests on 69 samples of GC liver metastases. Masson's trichrome and H&E staining analyses demonstrated a prevalence of thick ECM in most tumor metastatic niches and predicted poor prognosis. Immunostaining results indicated that abundant ECM components primarily originated from CAFs and were crosslinked by LOX. This underscores the supportive roles of increased TME stiffness in the progression of GC liver metastasis.

In this study, we identified through RNA-seq analysis that Troponin T1, slow skeletal type (*TNNT1*) is significantly upregulated in tumor cells under the influence of high ECM stiffness. Though limited in tumor related studies, *TNNT1* has been previously implicated in breast cancer and colorectal cancer progression [23, 24]. Comparing its expression levels between GFP^{+}/$mCherry^{+}$ (dormant) and $mCherry^{+}$ (activated) cells, we observed upregulated TNNT1 expression in activated tumor cells under ECM stiffness pressure. This suggests that TNNT1 served as a specialized mechanosensitive molecule, rapidly expressed by tumor cells in response to significant external mechanical pressures and potentially participated in dormancy-awakening mechanisms. We also propose a novel therapeutic strategy targeting LOX through TNNT1 as a measure of ECM stiffness.

2 Materials and methods

2.1 Clinical samples

This study involved the collection of clinical samples from gastric cancer (GC) patients at Renji Hospital, affiliated with Shanghai Jiaotong University. All procedures were approved by the Ethics Committee of Renji Hospital, and informed consent was obtained from each participant.

The study comprised two primary cohorts. Cohort I included 69 cases of GC liver metastasis, organized for H&E staining, Masson's trichrome staining and tumor microarray (TMA) analysis. Cohort II consisted of 24 cases of frozen liver metastasis tissue collected within the last five years. Cohort II was utilized for immunofluorescence staining, and atomic force microscopy (AFM) measurement. All samples from Cohort II were extracted for total RNA and proteins for experiments. All patients were diagnosed by clinical surgeons and professional pathologists. The Ethics Committee approval for this study was documented under No. RA-2019-116.1.

2.2 Animal experiments

In this study, we utilized male C57BL/6J mice aged 6 to 8 weeks, which were procured from East China Normal University. For the establishment of the *Trp53*$^{R172H/+}$/*Cdh*$^{fl/fl}$/*Atp4b*-Cre (TPA) spontaneous GC mouse model, lox-stop-lox-*Trp53*$^{R172H/+}$ mice were obtained from Jackson Laboratories, while *Cdh*$^{fl/fl}$ and *Atp4b*-Cre mice were sourced from Cyagen Technologies. All experimental protocols and animal handling procedures were reviewed and approved by the Research Ethics Committee of East China Normal University. We adhered to the guidelines set forth by the National Academy of Sciences in the "*Guide for the Care and Use of Laboratory Animals*," ensuring that all animals were appropriately housed and cared for throughout the study. The approved protocol number for the animal experiments conducted is 20,141,204, as assigned by the Research Ethics Committee of East China Normal University.

TPA mice were respectively treated with IgG, LOX mAb or BAPN every 3 days at 10 months. After establishment of the model, it was used to demonstrate the link between ECM stiffness and *Tnnt1*.

2.3 Atomic force microscopy (AFM) measurement

To accurately measure the stiffness of tissue, we used the atomic force microscope (FastScan Bio, Bruker, USA) at the Instrumental Analysis Center, Shanghai Jiao Tong University.

Freshly prepared tissues ensure a smooth surface and are thoroughly rinsed in PBS to remove residual impurities. They are then carefully affixed to the surface of a microscope slide using optically adhesive glue to ensure optimal flatness and stability during imaging. Place the prepared tissue samples on the stage and configure the machine program to allow the probe to contact the tissue at 100 μm intervals within a grid of 400 μm × 500 μm, obtaining force curves. Using software (NanoScope_Analysisto) process the force curves, the elastic modulus at each location is obtained, thereby elucidating the stiffness of the respective samples.

2.4 Establishment of the dormancy-awakening system

The CDK-binding region of p27 was mutated and fused with the GFP protein as a marker. Meanwhile, mCherry was stably transfected into tumor cells as a tumor cell indicator. After transfection, treat the cells with serum-free medium to induce a quiescent state. Then apply serum activation, and collect samples at various time points to measure the expression levels of GFP. Concurrently, the expression levels of the cell cycle protein gene CCND1 were assessed, and expression curves over time were plotted. It was confirmed that the expression curve of GFP was completely opposite to that of CCND1, demonstrating the success of the system.

2.5 In vivo liver metastatic models

To evaluate the impact of the stiffness of the hepatic metastatic microenvironment on dormant tumor cells in vivo, we established a liver metastasis mouse model via intrasplenic injection of the murine GC cell line MFC$^{mCherry/GFP-p27K-}$. Firstly, male C57BL/6J mice were anesthetized by 2.5% isoflurane for performing a surgical intervention. Then, the right abdominal cavity was carefully sectioned and the spleen was completely exposed. An insulin syringe was employed for the intrasplenic injection and the murine GC cell line MFC which was prepared at a concentration of 2×10^6 cells suspended in 2μL of phosphate-buffered saline (PBS) per mouse was injected into the spleen for 10 s. Following the injection, the abdominal incision was meticulously closed using sutures and disinfected with medical-grade alcohol. The mice were then placed on a 37 °C warming pad until they woke up.

There were 4 cohorts of liver metastasis mouse models used for several designs in this study. C57BL/6J mice injected intrasplenically with MFC$^{mCherry/GFP-p27K-}$ cells were designated as Cohort I. Cohort I was utilized to evaluate the p27K- cell dormancy detection system, enabling the differentiation of active (mCherry+) and dormant (GFP+/mCherry+) niches in vivo.

In cohort II, C57BL/6J mice were injected with MFC-$^{mCherry/GFP-p27K-}$ cells and activated hepatic stellate cells (aHSCs) (5×10^5 cells in 20μL PBS) and subsequently treated with either PBS or BAPN (100 mg/kg via intraperitoneal injection daily). Following the treatment, the mice were utilized for survival analysis, CT & Imaging, IHC & IF detection and AFM measurement to demonstrate how ECM stiffness affects tumor dormancy.

In order to filter out the key genes associated with ECM stiffness and activation of tumor cells via RNA-seq, the mice in cohort III were divided into two groups. One group received an intrasplenic injection of MFC$^{mCherry/GFP-p27K-}$ cells, while the other group was injected with a mixture of MFC$^{mCherry/GFP-p27K-}$ cells and aHSCs. Subsequently, dormant cells and active cells were selected by flow cytometry for analysis.

In Cohort IV, the mice were injected intraperitoneally with PBS or carbon tetrachloride (0.5 μl/g, in 25% olive oil, every 3 days) for a 20 day's pretreatment. The two groups of pre-treated mice were injected with MFC-$^{mCherry/GFP-p27K-}$-sh*Tnnt1* or MFC$^{mCherry/GFP-p27K-}$-shCtrl in

spleen respectively. Following modeling, these mice were used for survival analysis, CT & Imaging, IHC & IF detection. Meanwhile, expression level of ECM protein-related genes, proliferation-related genes and matrix stiffness were measured at different time points (20, 25, 35 days).

2.6 CT-combined 3D organ reconstruction bioluminescence imaging

A combined approach of bioluminescence imaging and computed tomography (CT) was utilized to monitor liver metastasis formation and progression in mouse models. Following the intraperitoneal injection of 150 mg D-luciferin (Promega), the mice were anesthetized with 2.5% vaporized inhaled isoflurane. In Vivo Imaging System (IVIS) Spectrum (Caliper Life Sciences, USA) was used for imaging the metastatic niches in liver. Meanwhile, organ reconstruction in mouse models was performed by CT system. Then CT images were merge with bioluminescence signals to enhance the accuracy of lesion localization and organ reconstruction. Post-imaging, the mice were euthanized, and their livers were isolated for exclusive imaging to minimize potential imaging errors. The entire imaging and reconstruction process was facilitated by the Living Image software (version 4.5.3), which enabled standardized quantification and automated organ reconstruction.

2.7 Cell culture and reagents

Human GC cell lines NCI-N87, BGC-823 and AGS were sourced from the Shanghai Cancer Institute, Renji Hospital, Shanghai Jiao Tong University School of Medicine. The murine GC cell line MFC was obtained from the Cell Bank of the Chinese Academy of Sciences. All cell lines were cultured in RPMI 1640 medium supplemented with 10% fetal bovine serum (FBS) and 1% antibiotic solution, maintaining an incubation environment of 37 °C with 5% CO2.

2.8 Immunohistochemistry (IHC) and immunofluorescence (IF)

In order to demonstrate TNNT1 expression in extracellular matrix (ECM) enriched or deficient metastatic niches, we utilized paraffin sections of human gastric cancer (GC) liver metastasis tissues and mouse liver metastasis tissues for validation at the tissue level. We employed immunohistochemistry (IHC) and immunofluorescence (IF) staining to ascertain the expression profiles of proteins of interest.

For the IHC procedure, the prepared slides were first deparaffinized in xylene and then rehydrated through a gradient series of alcohol (100–95–85–75%). Antigen retrieval was conducted using citrate buffer at 95 °C for 15 min. Subsequently, the tumor tissues were treated with 0.3% hydrogen peroxide in methanol to quench endogenous peroxidases. After a one-hour blocking step in 10% bovine serum albumin (BSA), the slides were incubated with specific primary antibodies overnight at 4 °C. This was followed by an incubation with the corresponding horseradish peroxidase (HPR)-conjugated secondary antibody, diluted at 1:300. The localized proteins were visualized with 3,3'-diaminobenzidine (DAB) chromogen (product number 8059 from Cell Signaling Technology, USA) under a microscope after the slides were counterstained with hematoxylin. Additionally, standard hematoxylin and eosin (H&E) staining was performed according to established protocols.

For tissue-level immunofluorescence staining, the initial slide preparation steps were identical up to the antigen retrieval phase. The slides were then blocked with 10% BSA for one hour and incubated with the primary antibodies overnight at 4 °C. The target proteins were labeled with the corresponding secondary antibodies conjugated to green and red fluorescent dyes and incubated for one hour at room temperature. Nuclei were stained with DAPI following established procedures, prior to capturing digital images with a confocal microscope. For cell-based immunofluorescence staining, cells were cultured on chamber slides and fixed with 4% formaldehyde. Cells were permeabilized with 0.2% Triton X-100 or left unpermeabilized for membrane proteins. The subsequent steps, from blocking to protein labeling, mirrored those used in tissue immunofluorescence staining. Digital images were captured using a confocal microscope.

In order to detect activated and dormant cells, we employed immunofluorescence (IF) staining to ascertain the expression profiles of proteins within cells. For cell-level immunofluorescence staining, standard clean coverslips were soaked in 75% ethanol, then dried under a sterile laminar flow hood and placed in 6-well, 12-well, or 24-well plates. Cells were seeded with culture medium and incubated overnight to achieve approximately 30–60% confluence. After treatment according to specific experimental requirements, the culture medium was aspirated, and the cells were washed twice with PBS. The cells were fixed with 4% formaldehyde for 15 min at room temperature. The fixative was removed, and the cells were washed three times with PBS for 5 min each, with gentle shaking. Cells were permeabilized with 0.2% Triton X-100 for 5 min at room temperature, then washed three times with PBS for 5 min each, with gentle shaking. Samples were blocked with blocking solution for 60 min at room temperature. The blocking solution was aspirated, and the primary antibody was added. After incubation for 60 min at room temperature or overnight at 4 °C with gentle shaking, the primary antibody was removed, and the cells were washed three

times with PBS for 5 min each, with gentle shaking. The cells were then incubated with the diluted fluorescent secondary antibody for 40 min at room temperature in the dark with gentle shaking. Excess antibody was removed, and the cells were washed three times with PBS for 5 min each, with gentle shaking. DAPI was added and incubated in the dark for 5 min. Excess DAPI was washed off with four changes of PBS for 5 min each. The coverslips were gently blotted dry with filter paper, and a drop of anti-fade mounting medium (a 1:1 mixture of PBS and glycerol) was placed on a slide. The coverslip with the cells was carefully placed cell-side down onto the drop, avoiding air bubbles. The cells were observed for green fluorescence under a fluorescence microscope.

2.9 Quantitative real-time PCR

Total RNA was extracted from the samples using Trizol reagent (15,596,026, Ambin, CA, USA), and the RNA samples were then reverse transcribed into cDNA using the PrimeScript RT-PCR kit (RR037A, Takara, Japan), following the manufacturer's protocols. Quantitative real-time PCR was performed to analyze the expression of the genes of interest using the 7500 Real-time PCR system (Applied Biosystems, USA). The detection system was constituted with SYBR Premix Ex Taq (04,913,914,001, Roche). The relative mRNA expression levels were determined, with 18 S rRNA serving as an endogenous control to normalize the data. Sequences of primers are as follows:

Genes	Forward	Reverse
Acta2	GTCCCAGACATCAGGGAGTAA	TCGGATACTTCAGCGTCAGGA
Lox	TCTTCTGCTGCGTGACAACC	GAGAAACCAGCTTGGAACCAG
Col1a1	GCTCCTCTTAGGGGCCACT	ATTGGGGACCCTTAGGCCAT
Mki67	ATCATTGACCGCTCCTTTAGGT	GCTCGCCTTGATGGTTCCT
Ccnd1	TGACTGCCGAGAAGTTGTGC	CTCATCCGCCTCTGGCATT

2.10 Transduction of short-hairpin RNA and construction of lentivirus

The lentivirus carrying short-hairpin RNA (shRNA), sh*TNNT1*, *shTnnt1* and a negative control (shCtrl) were constructed by Genechem Co., Ltd. (Shanghai) to facilitate stable knockdown of *TNNT1* in human GC cells and *Tnnt1* in murine GC cells. Upon reaching 40-50% confluence, GC cells were subjected to lentiviral transduction in the presence of 8 μg/ml Polybrene (H9268; Sigma-Aldrich, St. Louis, MO). To select for cells with stable knockdown, the virally infected cells were cultured in medium containing 5 μg/ml puromycin (A1113802, Gibco, USA). The efficiency of transduction was assessed through qRT-PCR and Western blotting.

2.11 Cell viability assay

Cell viability was assessed using the Cell Counting Kit-8 (CCK-8, Dojindo, Japan) to evaluate the proliferative capacity and apoptosis rates of GC cell lines subjected to genetic and environmental modifications. We selected four GC cells for this experiment (NCI-N87, BGC-823, AGS, MFC). NCI-N87 was used to construct NCI-N87-shCtrl and NCI-N87-sh*TNNT1*, then these cells (5000 cells/100μl medium) were seeded into 96-well plates with different stiffness degrees (0.5 kPa, 4 kPa and 40 kPa). MFC was used to construct MFC-shCtrl and MFC-sh*Tnnt1*, then these cells (3000 cells/100μl medium) were seeded into 96-well plates with different stiffness degrees (0.5 kPa, 4 kPa and 40 kPa). BGC-823 and AGS were used to construct *TNNT1*-OE and NC groups, then these cells (3000 cells/100μl medium for BGC-823, 5000 cells/100μl medium for BGC-823) were seeded into 96-well plates with different stiffness degrees (0.5 kPa, 4 kPa and 40 kPa). After a one-hour incubation with CCK-8 reagent, diluted at a ratio of 1:10 in medium, absorbance was measured at 450 nm using a microplate reader at predetermined intervals. The detection was performed for independent three times with five repeating wells.

2.12 Western blotting

Total proteins from the four types GC cells (NCI-N87-shCtrl, NCI-N87-sh*TNNT1*, MFC-shCtrl and MFC-sh*Tnnt1*) were extracted using IP-lysate buffer (P70100, NCM Biotech, China), and protease and phosphatase inhibitors (P002, NCM Biotech, China) were added to prevent degradation and dephosphorylation. After incubation, the lysates were centrifuged at 4 °C for 15 min to obtain the supernatant. Protein concentration was measured by BCA Protein Assay Kit (Pierce Biotechnology, USA), and 10 μg of each sample was separated by SDS-PAGE on 8–10% polyacrylamide gels, followed by transfer to nitrocellulose membranes. The membranes containing the transferred proteins were blocked with 5% non-fat dry milk for 1 h to minimize nonspecific binding. They were then incubated with primary antibodies overnight at 4 °C. Finally, protein bands were detected using an HRP-conjugated secondary antibody, then membranes were visualized with ECL reagent solution by the Bio-Rad system. The antibodies involved here were as follows: TNNT1 (ab155028, Abcam, 1:1000), Cyclin D1 (ab134175, Abcam, 1:10,000), Cyclin E1 (ab33911, Abcam, 1:1000),

Cyclin E2 (ab40890, Abcam, 1:5000), p-Rb (ab184796, Abcam, 1:1000), Rb (ab181616, Abcam, 1:2000), Tubulin (11224-1-AP, Proteintech, 1:5000), and corresponding HRP-conjugated secondary antibodies (SA00001-1 and SA00001-2, Proteintech, 1:5000 both).

2.13 Reagents

The following antibodies uesd in the experiment were purchased from Abcam: α-SMA (ab7817), CK19 (ab52625), Collagen I (ab138492), mCherry (ab167453), GFP (ab6556), KI67 (ab16667), LOX (ab174316). *TNNT1* Polyclonal Antibody (AB_2853518) was purchased from Thermo Fisher Scientific. BAPN was purchased from SigmaAldrich.

3 Results

3.1 Upregulation of stiffness in liver metastatic sites leads to poor prognosis

We first evaluated the histomorphological features of GC liver metastatic niches via H&E staining (Fig. 1A) and Masson's trichrome staining (Fig. 1B) to confirm the enrichment degree of the extracellular matrix (ECM). Results have shown that at the metastasis site, enrichment of ECM and multiple niches could be observed, which forming a complex tumor microenvironment (TME). Data illustrated that larger metastatic niche (with diameter > 800 μm) could be found in ECM enriched metastasized livers compared to those in ECM deficient ones (Fig. 1C and D, Supplementary Fig. 1A-1B). To further consolidate, we used atomic force microscopy (AFM) to assess the overall stiffness of livers with metastatic niches of GC and results demonstrated that ECM enriched livers with metastatic niches exhibited significantly higher stiffness (Fig. 1E). Moreover, the prognosis of GC patients with ECM enriched liver metastases is significantly poorer (Fig. 1F). Thus we continued to investigate the primary components of ECM in liver metastatic niches of GC. IF staining and RNA-scope identified three vital components: α-SMA expressed by cancer associated fibroblasts (CAFs); CAFs derived collagen I, a crucial component in the TME which deposited around niches; and LOX, which is responsible for performing crosslinks among various collagen fiber bundles (Fig. 1G and H). Multiple IF followed by QuPath analysis further confirmed these findings: the enrichment of α-SMA positive CAFs, CAFs derived collagen I together with overexpression of LOX led to upregulation of stiffness of liver metastatic niches (Fig. 1I and J).

Fig. 1 Stiffness of metastatic niche affects the prognosis of GC. (**A-B**) Shown are H&E staining (**A**) or Masson's trichrome staining (**B**) on GC liver metastasis with enriched or deficient extracellular matrix (ECM) and displaying the distribution of which. Scale bars, 500 μm (3 repeats performed per tissue, 3 fields assessed per sample). (**C-D**) Numbers of metastatic niches at different diagrams in ECM enriched or deficient metastasized livers are depicted ($n = 69$ cases). (**E**) Atomic force microscopy (AFM) measurements of stiffness (Young's modulus) of metastatic niches with varying ECM abundance ($n = 12$ cases per group). (**F**) Survival curves illustrating the impact of ECM abundance on prognosis in GC patients with liver metastasis ($n = 69$). (**G**) Immunofluorescence (IF) staining demonstrating the composition of ECM proteins in GC liver metastasis samples (3 repeats performed per tissue, 3 fields assessed per sample); blue, DAPI; green, CK19; red, α-SMA (upper), Collagen I (middle), LOX (lower); scale bars, 500 μm. (**H**) RNA in situ hybridization (RNAscope) displays mRNA expression levels and distributions of *ACTA2* (upper), *COL1A1* (middle), and *LOX* (lower) in GC liver metastasis samples (3 repeats performed per tissue, 3 fields assessed per sample); scale bar: 25 μm. (**I-J**) Multiple immunofluorescence (mIF) (**I**) and Qupath analysis (**J**) showing the expressions and distributions of ECM proteins in liver metastasis of high or low stiffness (3 repeats performed per tissue, 3 fields assessed per sample); blue, DAPI; green, collagen I; red, α-SMA; orange, LOX; cyan, CK19; scale bars, 250 μm

Taken together, these results have demonstrated that elevated ECM stiffness at liver metastasis predicts poor prognosis of GC.

3.2 TME of high stiffness promote dormant tumor cells to awake

To explore how stiffness of TME affect on tumor dormancy, we then construct the dormancy-awakening system. Metastatic tumor cells may enter a dormant state due to nutrient deprivation, adaptation challenges in alien environments, or immune cell attacks, etc. Cyclin-dependent kinase (CDK) inhibitor, p27 would exist to hamper the expressions and functions of various cell cycle related genes and degenerate at G1 phase (Fig. 2A). We next constructed a GFP-fused mutant protein $p27K^{-}$ lacking CDK inhibitory activity to recognize the dormant tumor cells and used mCherry to mark all tumor cells (Fig. 2B). Real-time PCR has shown that the expression of *GFP* and *CCND1* demonstrated opposing trends across the cell cycle, aligning with our experimental design and indicating the efficacy of this system (Fig. 2C). We have also assessed this system via in vivo intrasplenic injection liver metastasis mouse model using murine GC cell line MFC to distinguish the active niches ($mCherry^{+}$) or dormant niches (GFP+/mCherry+) (Fig. 2D). To unveil how ECM stiffness affected the tumor dormancy in liver metastasis, we separated CAFs from liver metastasis of intrasplenic injection mouse model and performed another injection using mixture of CAFs and MFC cell line followed by administration of LOX inhibitor BAPN (Fig. 2E). AFM measurement has illustrated

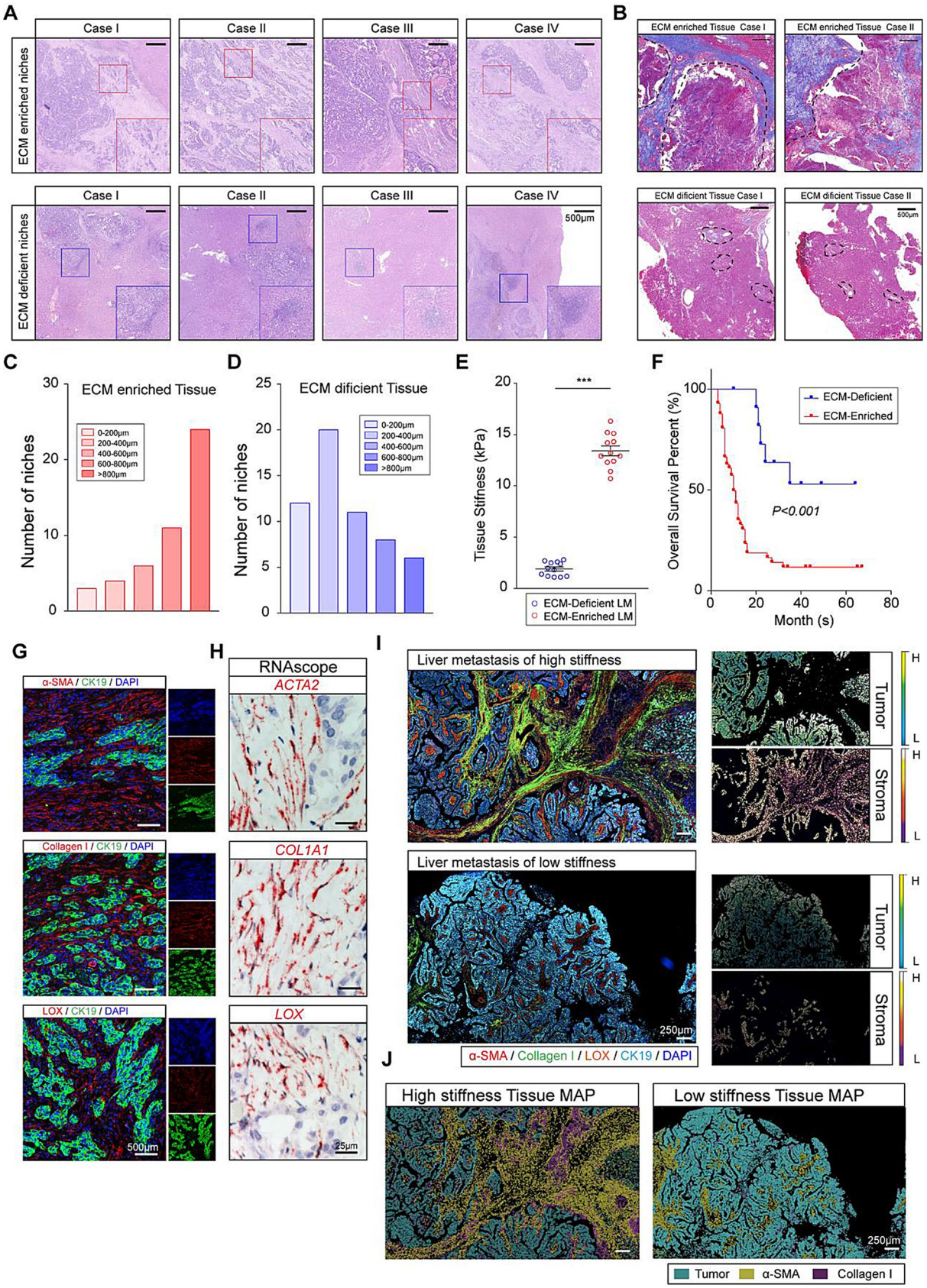
A
Case I
Case II
Case III
Case IV
ECM enriched niches
ECM deficient niches
500μm
B
ECM enriched Tissue Case I
ECM enriched Tissue Case II
ECM dificient Tissue Case I
ECM dificient Tissue Case II
C
ECM enriched Tissue
Number of niches
0-200μm
200-400μm
400-600μm
600-800μm
>800μm
D
ECM dificient Tissue
E
Tissue Stiffness (kPa)
***
ECM-Deficient LM
ECM-Enriched LM
F
Overall Survival Percent (%)
ECM-Deficient
ECM-Enriched
P<0.001
Month (s)
G
α-SMA / CK19 / DAPI
Collagen I / CK19 / DAPI
LOX / CK19 / DAPI
500μm
H
RNAscope
ACTA2
COL1A1
LOX
25μm
I
Liver metastasis of high stiffness
Liver metastasis of low stiffness
Tumor
Stroma
H
L
250μm
α-SMA / Collagen I / LOX / CK19 / DAPI
J
High stiffness Tissue MAP
Low stiffness Tissue MAP
250μm
Tumor
α-SMA
Collagen I

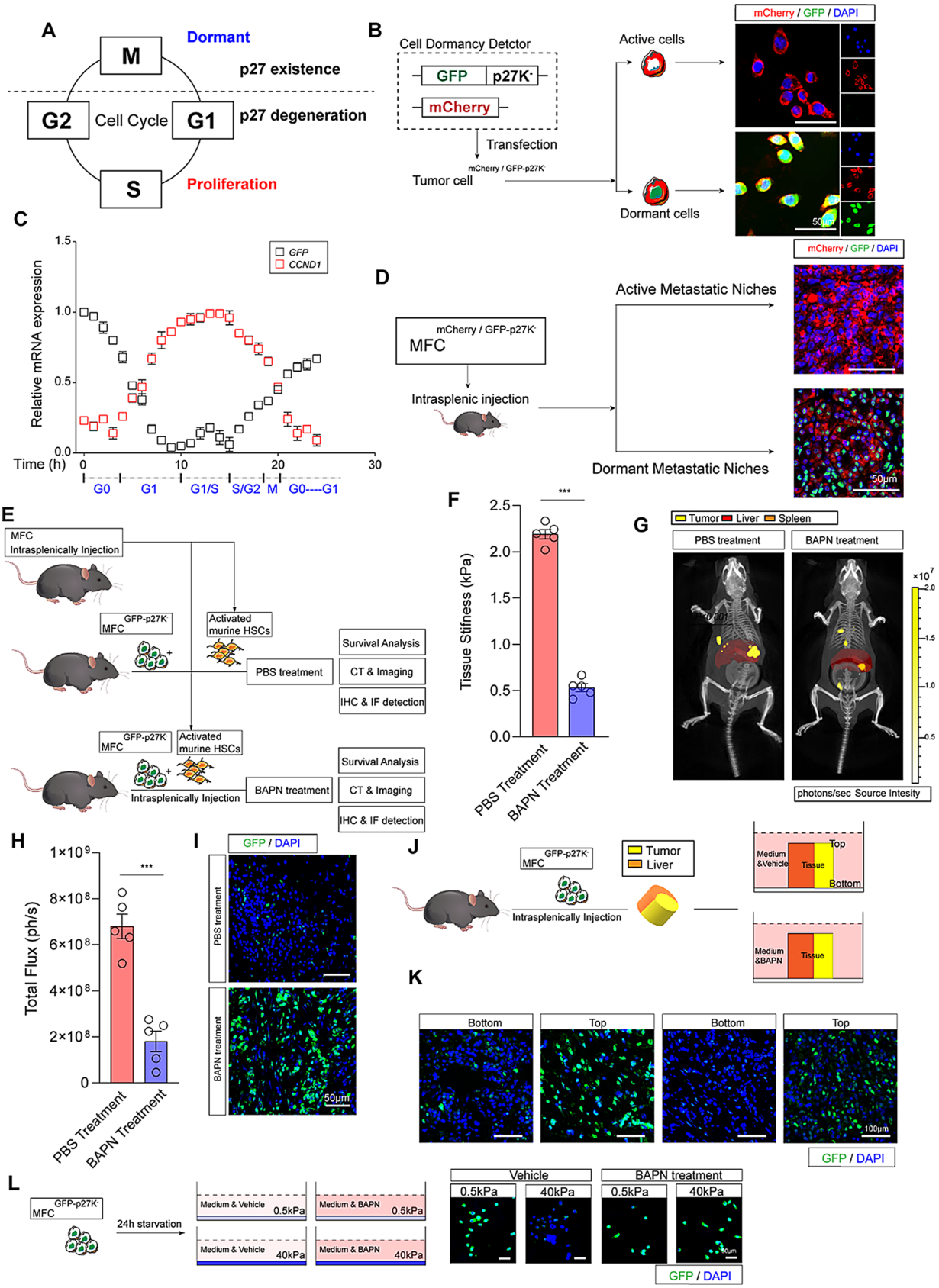
A
M
Dormant
p27 existence
G2
Cell Cycle
G1
p27 degeneration
S
Proliferation
B
Cell Dormancy Detctor
GFP
p27K-
mCherry
Transfection
mCherry / GFP-p27K-
Tumor cell
Active cells
Dormant cells
mCherry / GFP / DAPI
50μm
C
GFP
CCND1
Relative mRNA expression
Time (h)
G0
G1
G1/S
S/G2
M
G0----G1
D
mCherry / GFP-p27K-
MFC
Intrasplenic injection
Active Metastatic Niches
Dormant Metastatic Niches
mCherry / GFP / DAPI
50μm
E
MFC
Intrasplenically Injection
GFP-p27K-
Activated murine HSCs
PBS treatment
BAPN treatment
Survival Analysis
CT & Imaging
IHC & IF detection
F
Tissue Stifness (kPa)
***
PBS Treatment
BAPN Treatment
G
Tumor
Liver
Spleen
PBS treatment
BAPN treatment
×10^7
photons/sec Source Intesity
H
Total Flux (ph/s)
***
PBS Treatment
BAPN Treatment
I
GFP / DAPI
PBS treatment
BAPN treatment
50μm
J
GFP-p27K-
MFC
Intrasplenically Injection
Tumor
Liver
Medium &Vehicle
Tissue
Top
Bottom
Medium &BAPN
K
Bottom
Top
Bottom
Top
100μm
GFP / DAPI
L
GFP-p27K-
MFC
24h starvation
Medium & Vehicle
0.5kPa
Medium & BAPN
0.5kPa
Medium & Vehicle
40kPa
Medium & BAPN
40kPa
Vehicle
BAPN treatment
0.5kPa
40kPa
0.5kPa
40kPa
GFP / DAPI

Fig. 2 ECM stiffness is closely related with tumor awakening progress. (**A**) Schematic diagram illustrating cell cycle stages and the principle of p27K⁻ cell dormancy detection system. (**B**) Schematic diagram depicting the composition of the p27K⁻ cell dormancy detection system followed by confirmation via IF staining detecting the activated cells and dormant cells; blue, DAPI; green, GFP; red, mCherry; scale bar, 50 μm. (**C**) Differential expression of *GFP-p27K⁻* and *CCND1* during the cell cycle measured by real-time PCR. (**D**) IF staining on livers of mouse models intrasplenically injected with MFC cells expressing dormancy-awakening system to distinguish activated or dormant metastatic niches (3 repeats performed per tissue, 3 fields assessed per sample); blue, DAPI; green, GFP; red, mCherry; scale bar, 50 μm. (**E**) Schematic diagram illustrating the experimental strategy of intrasplenic injection of MFC cell line (dormancy-awakening system) mixed with activated hepatic stellate cells (HSCs), followed by therapeutic treatment with LOX inhibitor BAPN. (**F**) Changes in stiffness of metastasized livers after therapeutic administration of PBS or BAPN in intrasplenic injection mouse model ($n=5$ mice per group, mean ± s.e.m.; two tailed unpaired *t*-test). (**G-H**) CT combined 3D organ reconstruction bioluminescence imaging displaying tumor signals of mice bearing liver metastasis treated with PBS or BAPN. ($n=5$ mice per group, mean ± s.e.m.; two tailed unpaired t-test). Tumor signals, yellow; reconstructed liver, red; reconstructed spleen, orange. Scale color bar, 1.00×10^6-2.00×10^7. (**I**) IF staining measuring the GFP-P27K⁻ expression in metastasized livers of mouse models treated with PBS or BAPN (3 repeats performed per tissue, 3 fields assessed per sample); blue, DAPI; green, GFP; scale bar, 50 μm. (**J-K**) Ex-vivo experiments showing the effects of stiffness on liver metastasis of mouse model (3 repeats performed per tissue, 3 fields assessed per sample). blue, DAPI; green, GFP; scale bar, 100 μm. (**L**) IF staining studying matrix of different stiffnesses induced dormancy-awakening status detected by GFP-p27K- on MFC cell (3 repeats performed per tissue, 3 fields assessed per sample). blue, DAPI; green, GFP; scale bar, 100 μm

that BAPN treatment efficiently diminished the stiffness of liver metastasis (Fig. 2F). CT combined 3D organ reconstruction bioluminescence imaging further confirmed the results that high stiffness of liver metastasis significantly facilitated outgrowth of metastatic tumor cells (Fig. 2G and H). Furthermore, BAPN could also result in tumor dormancy in metastatic niches (Fig. 2I). Considering that LOX itself plays vital roles in tumorigenesis via directly promoting tumor cell proliferation, especially in liver metastasis of GC, we used ex vivo test to exclude. Mouse liver tissues containing tumor niches were sectioned in the middle before cultured in dishes to ensure both tissue sections exhibited identical histological features and TME. One section was positioned directly against the high-hardness bottom of the dish, while the other remained unexposed to the dish bottom (Fig. 2J). Data have deciphered that the administration of BAPN could not inhibit the bottom-stiffness induced activation of tumor cell but significantly increased the number of dormant tumor cells (Fig. 2K). Additionally, we have also performed in vitro study. MFC p27K⁻ cells were treated with FBS free medium followed by plantation on 0.5 kPa or 40 kPa gel coated dishes. Results have shown that stiffening stroma efficiently awakened dormant MFC cells and this effect could be hampered by BAPN treatment (Fig. 2L).

In summary, our data have shown that increasing ECM stiffness could stimulate the activation of dormant tumor cells at liver metastatic niches.

3.3 High ECM stiffness induces expression of *TNNT1*

We next set off to filter out the key genes involved in ECM stiffness and activation of tumor cells via combining the in vivo and in vitro RNA-seq. Troponin T1, slow skeletal type (*TNNT1*) was among the overlapping genes (Fig. 3A). Gene set enrichment analysis (GSEA) have also demonstrated that TNNT1 was involved in ECM related and cell cycle pathway (Supplementary Fig. 2A-2 C). To explore, we gained the metastasized livers of GC patients with high or low TNNT1 expression to measure the stiffness. AFM was utilized for measuring individual stiffness at 425 independent sites of every tissue and constructed a matrix to visualize the surface plot of tissue stiffness. Results have indicated that tissues with high *TNNT1* expression exhibited a greater number of high-stiffness points, forming several significant peaks of elevated stiffness (Fig. 3B and C). Consistently, the overall stiffness in TNNT1-H tissues is also higher than that in TNNT1-L ones (Fig. 3D). It has been reported that tissue stiffness is closely related to certain parameters of collagen proteins (e.g. length, width and enrichment). We first investigated the collagen abundance using picrosirius red, data showed high expression of TNNT1 in tissue is closely related to large amounts of collagens (Fig. 3E). These findings were also in consistence with results of mIF (Fig. 3F). Furthermore, we used CT FIRE system to analyze the parameters of collagen fibre. Results have unveiled that TNNT1-H liver metastatic tissues contained significantly more fibres, each of which was also longer and wider (Fig. 3G and J). Notably, the co-efficient of variation index of high TNNT1 expressed tissues is smaller, which indicates more consistent collagen alignment and higher cross-linking (Fig. 3K). What's more, the expression of TNNT1 in tumor cells exhibits an inverse relationship with the distance from regions enriched with collagen fibres (Fig. 3L and M).

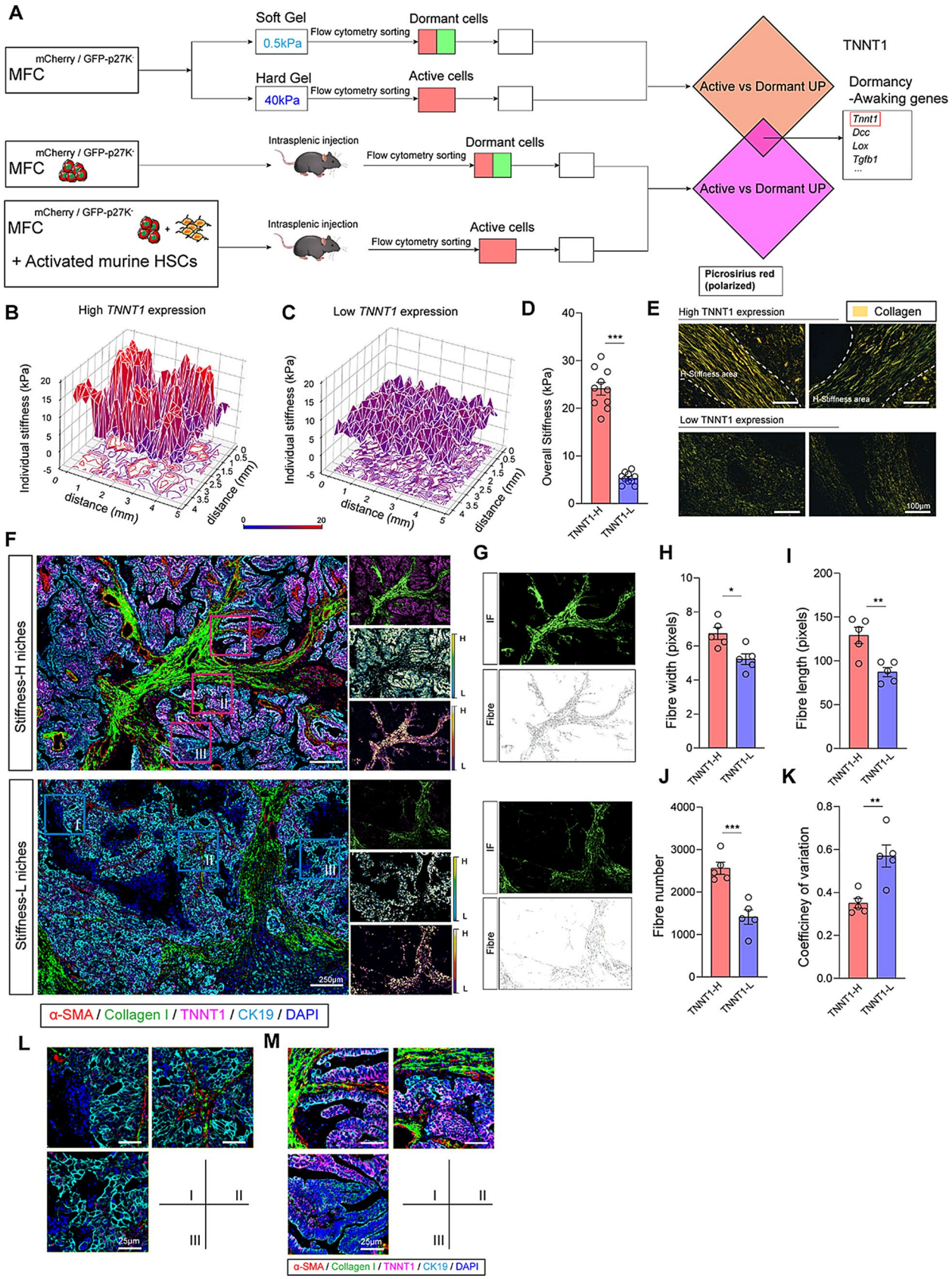
A
Soft Gel
0.5kPa
Flow cytometry sorting
Dormant cells
Hard Gel
40kPa
Flow cytometry sorting
Active cells
mCherry / GFP-p27K-
MFC
Intrasplenic injection
Flow cytometry sorting
Dormant cells
mCherry / GFP-p27K-
MFC
+ Activated murine HSCs
Intrasplenic injection
Flow cytometry sorting
Active cells
Active vs Dormant UP
Active vs Dormant UP
TNNT1
Dormancy
-Awaking genes
Tnnt1
Dcc
Lox
Tgfb1
Picrosirius red
(polarized)
B
High TNNT1 expression
Individual stiffness (kPa)
distance (mm)
C
Low TNNT1 expression
Individual stiffness (kPa)
distance (mm)
D
Overall Stiffness (kPa)
TNNT1-H
TNNT1-L
E
High TNNT1 expression
Collagen
H-Stiffness area
Low TNNT1 expression
100μm
F
Stiffness-H niches
Stiffness-L niches
250μm
α-SMA / Collagen I / TNNT1 / CK19 / DAPI
G
IF
Fibre
H
Fibre width (pixels)
I
Fibre length (pixels)
J
Fibre number
K
Coefficiney of variation
L
M
25μm
α-SMA / Collagen I / TNNT1 / CK19 / DAPI

Fig. 3 ECM stiffness triggers the upregulation of TNNT1 in metastatic tumor cells. (**A**) Procedure of RNA-seq to filter out genes related to tumor dormancy and ECM stiffness. (**B-C**) Measurements on individual stiffness of multiple points in metastasized livers of GC patients with high or low expressions of *TNNT1*. (**D**) Measurements on overall stiffness of metastasized livers of GC patients ($n = 10$ cases per group, mean ± s.e.m.; two tailed unpaired t-test). (**E**) Shown is picrosirius red (polarized) staining detecting the ECM remodeling in liver metastasis with high or low *TNNT1* expressions. (**F**) Shown are mIF staining displaying the relationship between ECM stiffness and TNNT1 expressions in liver metastatic niches of GC patients (3 repeats performed per tissue, 3 fields assessed per sample). blue, DAPI; green, collagen I; red, α-SMA; purple, TNNT1; cyan, CK19; scale bars, 250 μm. (**G-K**) CT FIRE calculating the fibre data including width (**H**), length (**I**), number (**J**) and variation (**K**) in tissues with different expressions of TNNT1 ($n = 5$ patients per group, mean ± s.e.m.; two tailed unpaired t-test). (**M-N**) Different fields from (**F**) showing the relationship of TNNT1 and distance from ECM

To summarize, we have elucidated that TNNT1 was induced by high stiffness of ECM.

3.4 TNNT1 expression in liver metastasis of high stiffness predicts poor prognosis

To set off, we consolidate our previous results by conducting IF and IHC-P staining in GC liver metastatic niches, revealing TNNT1 localization within tumor cells, notably upregulated in ECM enriched metastatic niches (Fig. 4A). Subsequent investigation of fresh samples from GC liver metastases identified high *TNNT1* mRNA expression in ECM enriched liver metastases, positively correlating with overall tissue stiffness (Fig. 4C and D), in accordance with former results (Fig. 3D). Further survival analysis indicated that elevated TNNT1 expression predicts poorer patient prognosis (Fig. 5E). To further elucidate the relationship between TNNT1 and ECM stiffness, we scored TNNT1 and ECM stiffness related proteins according to staining in 69 GC liver metastasis sections, categorizing the level of which into None, Weak, Moderate, and Positive grades. Results demonstrated a close association between TNNT1 expression and ECM thickness (Fig. 4F), as well as significant positive correlations with α-SMA, Collagen I, and LOX expression (Fig. 4G and I). Moreover, harder metastatic niches showed significantly increased Ki67-positive cells, indicating higher proliferation activity with increased stiffness (Fig. 4J and K). Subsequent Ki67 staining of high and low TNNT1-expressing metastatic niches illustrated that elevated TNNT1 expression is positively correlated with the proliferative ability of tumor cells. (Figure 4L and M).

Collectively, we used clinical samples to illustrate ECM stiffness upregulated TNNT1 lead to poor prognosis.

3.5 Targeting ECM stiffness is effective to prohibit TNNT1-mediated activation of dormant tumor cells

We thus utilized a GC mouse model *Trp53*$^{R172H/+}$/*Cdh*$^{fl/fl}$/*Atp4b*-Cre (TPA) with spontaneous liver metastasis at a time point of about 10 months (the distance metastasis rate is approximate 90% and liver metastasis rate is 60%), and administrated LOX mAb or BAPN to prevent collagen fibres from cross-linking (Fig. 5A). The administration of mAb or BAPN significantly reduced the number of niches in liver or peritoneum (Supplementary Fig. 2D-2E). Results have elucidated that the administration of LOX mAb and BAPN significantly reduced the individual stiffness of metastasized liver in TPA mouse model (Fig. 5B and D). The enrichment of collagen I were also decreased in LOX mAb or BAPN treated mice (Fig. 5E). Furthermore, treatment caused decreasing of numbers and elevation of co-efficiency of variation in collagen fibres, which indicating abolished cross-linkling and diminished tissue stiffness (Fig. 5G and H). Consistently, the distribution and expression of TNNT1 significantly decreased due to downregulation of ECM stiffness via anti-LOX treatment according to either IF staining (Fig. 5I) or real-time PCR (Fig. 5J). We also performed an intrasplenic injection mouse model to further consolidate these results and IF have displayed attenuated TNNT1 expression in metastatic niches (Fig. 5K and L). At last, we also using MFC cells stably transfected with dormancy-awakening system for further study (Fig. 5M). Data have demonstrated that high expression of TNNT1 was related to less dormant tumor cells in tumor niches (Fig. 5N and O).

Taken together, our results have unveiled that BAPN or LOX mAb significantly reduced TNNT1 expression via decreasing ECM stiffness thus inhibit tumor activation.

3.6 TNNT1 triggers cell cycle and facilitates tumor cell activation

We initially performed intrasplenic injection for liver metastasis model, administering dormancy-awakening system transfected MFC cells alone or a mixture of which with aHSCs (Fig. 6A). Results indicated that the addition of aHSCs increased the stiffness of liver metastatic niches in mice, significantly reducing their survival (Fig. 6B). Further CT combined 3D organ reconstruction bioluminescence imaging showed the same trend (Fig. 6C and D). IF staining revealed fewer dormant tumor cells and significantly increased activated cells in mixture injection group (Fig. 6E

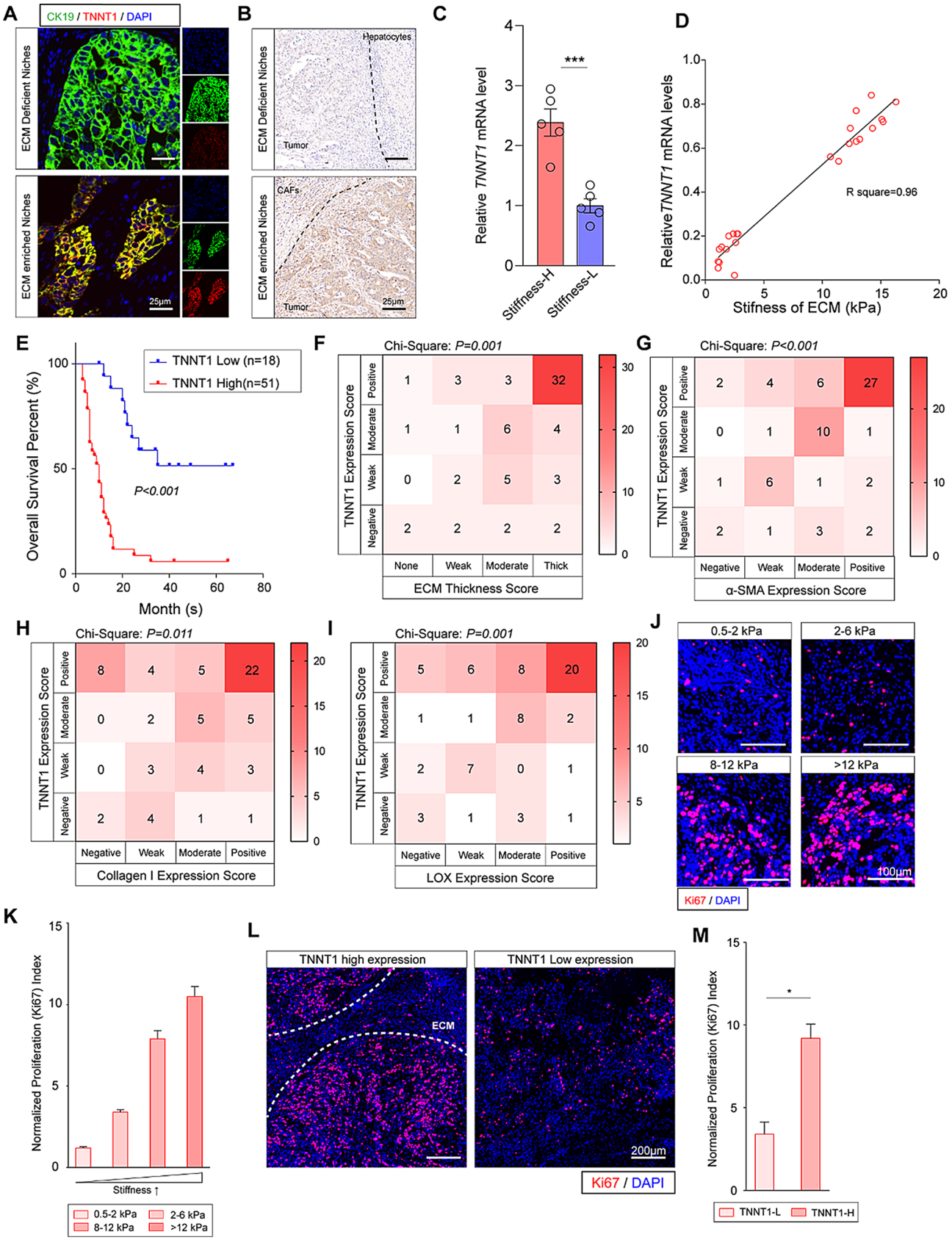
A
CK19 / TNNT1 / DAPI
ECM Deficient Niches
ECM enriched Niches
25μm
B
Hepatocytes
Tumor
CAFs
C
Relative TNNT1 mRNA level
***
Stiffness-H
Stiffness-L
D
Relative TNNT1 mRNA levels
R square=0.96
Stifness of ECM (kPa)
E
TNNT1 Low (n=18)
TNNT1 High(n=51)
Overall Survival Percent (%)
P<0.001
Month (s)
F
Chi-Square: P=0.001
TNNT1 Expression Score
Positive
Moderate
Weak
Negative
None
Weak
Moderate
Thick
ECM Thickness Score
G
Chi-Square: P<0.001
α-SMA Expression Score
H
Chi-Square: P=0.011
Collagen I Expression Score
I
Chi-Square: P=0.001
LOX Expression Score
J
0.5-2 kPa
2-6 kPa
8-12 kPa
>12 kPa
100μm
Ki67 / DAPI
K
Normalized Proliferation (Ki67) Index
Stiffness ↑
0.5-2 kPa
2-6 kPa
8-12 kPa
>12 kPa
L
TNNT1 high expression
TNNT1 Low expression
ECM
200μm
Ki67 / DAPI
M
Normalized Proliferation (Ki67) Index
*
TNNT1-L
TNNT1-H

Fig. 4 TNNT1 expression is related to high stiffness of ECM and predicts poor prognosis. (**A-B**) IF (**A**) and IHC-P (**B**) staining on GC liver metastases showing TNNT1 expression in ECM enriched or deficient metastatic niches (3 repeats performed per tissue, 3 fields assessed per sample); blue, DAPI; green, CK19; red, TNNT1; scale bar, 50 μm. (**C**) Real-time PCR measuring the *TNNT1* expressions in liver metastasis of high or low stiffness ($n=5$ patients per group, mean ± s.e.m.; two tailed unpaired t-test). (**D**) Correlation between ECM stiffness (kPa) and *TNNT1* expression levels detected by real-time PCR in 12 pairs of ECM enriched or deficient liver metastatic tissues. (**E**) Survival analysis on 69 cases GC patients with liver metastasis according to expression of TNNT1 ($n=69$). (**F-I**) Heatmaps illustrating correlations based on IF staining scores of TNNT1 expression with ECM thickness (**F**), α-SMA level (**G**), collagen I level (**H**), and LOX level (**I**) in 69 cases of GC liver metastasis. (**J-K**) IF staining showing the relationship between the number and distribution of Ki67-stained cells and tissue stiffness measured by AFM in GC liver metastases (3 repeats performed per tissue, 3 fields assessed per sample); blue, DAPI; red, Ki67; scale bar, 100 μm. (**L-M**) IF staining demonstrating the relationship between the number of Ki67-stained cells and TNNT1 expression levels in tumor cells within metastatic foci of gastric cancer liver metastases; blue, DAPI; red, Ki67; scale bar, 100 μm

and F). We thus interfered *Tnnt1* in dormancy-awakening system transfected MFC cells and pre-treated mice with carbon tetrachloride to induce abnormal activation of HSCs, resulting in increased ECM stiffness (Fig. 6G). Results showed that carbon tetrachloride treated mouse model exhibited significantly increased metastasis burden due to enhanced expression of ECM related genes, ECM stiffness and cell cycle genes, which could be reversed by knocking down *Tnnt1*, suggesting *Tnnt1* as a key effector gene promoting tumor cell awakening in response to increased ECM stiffness (Fig. 6H). CT combined 3D organ reconstruction bioluminescence imaging confirmed these findings (Fig. 6I and J). Meanwhile, we also found that fewer ECM components (PBS injection group) and *Tnnt1* knockdown could extend the survival period of mice, reducing the proliferation capacity of tumor cells (Fig. 6K and L).

In summary, the above results indicate that *TNNT1* is one of the key molecules promoting tumor cell awakening in response to increased ECM stiffness.

3.7 ECM stiffness induced TNNT1 provides potential therapeutic strategy for metastatic GC

We next evaluated the translational value of our findings. We first planted human GC liver metastasis derived cell line NCI-N87 and murine cell line MFC on gels of varying stiffness degrees (0.5 kPa, 4 kPa and 40 kPa) and extremely rigid plastic dishes. Results indicated that tumor cells on harder substrates exhibited stronger EdU staining, suggesting that high level of stiffness promotes tumor cell proliferation; this effect could be reversed by knockdown of *TNNT1* or *Tnnt1* (Fig. 7A). CCK-8 assays further corroborated these findings (Fig. 7B and C). Especially, no significantly differences in cell viability could be detected between *TNNT1* overexpression group and 40 kPa group, noting that TNNT1 is induced by high stiffness for gaining proliferation advantage (Figs. 6D and 7E). WB have also shown that TNNT1 is critical in cell cycle (Fig. 7F). To explore the clinical translational value of *TNNT1*, we used ex vivo test, we sampled tissues from GC patients with liver metastasis and cultured them in media with or without BAPN (Fig. 7G). IF staining revealed that tissues with high TNNT1 protein expression in tumor cells exhibited enhanced proliferation capacity and increased sensitivity to BAPN treatment, suggesting TNNT1 as a marker for cellular stiffness (Fig. 7H and I). We also constructed patient derived xenograft (PDX) mouse models, livers from GC patients containing $TNNT1^{+}$ niches with high stiffness and $TNNT1^{-}$ with low stiffness were performed (Fig. 7J). Results were in accordance with former conclusions that for metastatic niches with high TNNT1 protein level, reducing tissue stiffness using BAPN could yield favorable therapeutic outcomes (Fig. 7K and L).

Overall, these findings suggest TNNT1 as a novel marker for assessing ECM stiffness in GC liver metastasis tissues, with potential implications for guiding therapeutic strategies aimed at mitigating tumor progression (Fig. 7M).

4 Discussion

Metastasis microenvironment comprises critical components, including local cells in target organs, such as tumor associated macrophages (TAMs), lymphocytes, CAFs, and surrounding ECM [7, 11, 25, 26]. ECM as a critical role in TME, provides abundant nutrients and ample space for tumor cells to exchange substances and contact other TME cells. Moreover, ECM itself significantly supports tumor cell proliferation. In our observation and research using H&E or IF staining on clinical samples of GC liver metastasis, we found that large-diameter, deeply infiltrating, and

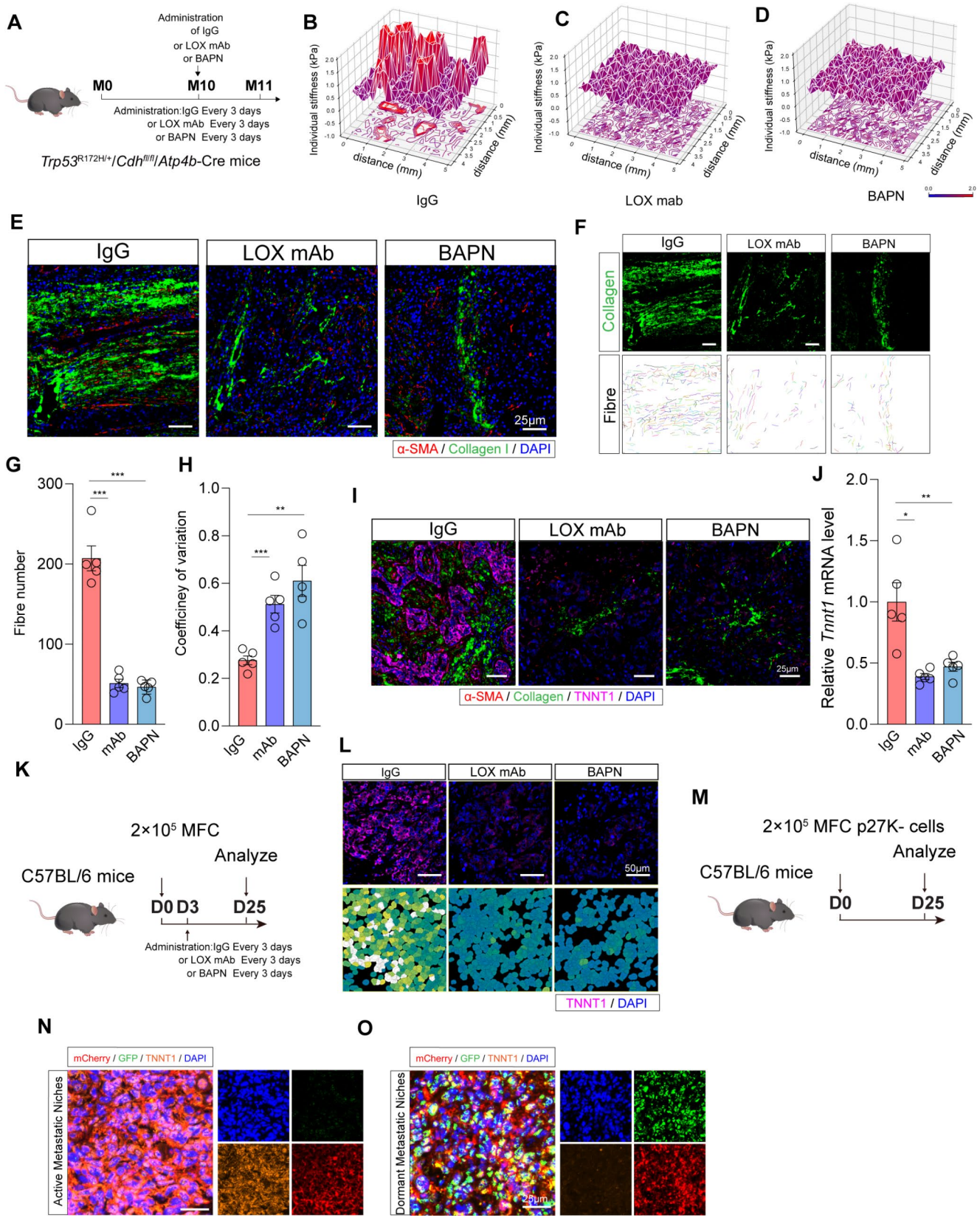
A
Administration of IgG or LOX mAb or BAPN
M0
M10
M11
Administration:IgG Every 3 days or LOX mAb Every 3 days or BAPN Every 3 days
Trp53R172H/+/Cdhfl/fl/Atp4b-Cre mice
B
C
D
Individual stiffness (kPa)
distance (mm)
IgG
LOX mab
BAPN
E
IgG
LOX mAb
BAPN
25μm
α-SMA / Collagen I / DAPI
F
Collagen
Fibre
G
Fibre number
H
Coefficiney of variation
I
α-SMA / Collagen / TNNT1 / DAPI
J
Relative Tnnt1 mRNA level
K
2×10⁵ MFC
Analyze
C57BL/6 mice
D0 D3 D25
Administration:IgG Every 3 days or LOX mAb Every 3 days or BAPN Every 3 days
L
50μm
TNNT1 / DAPI
M
2×10⁵ MFC p27K- cells
Analyze
C57BL/6 mice
D0 D25
N
mCherry / GFP / TNNT1 / DAPI
Active Metastatic Niches
O
mCherry / GFP / TNNT1 / DAPI
Dormant Metastatic Niches

Fig. 5 Stiffness induced TNNT1 overexpression confirmed by in vivo models. (**A**) Brief procedure displays *Trp53*$^{R172H/+}$/*Cdh*$^{fl/fl}$/*Atp4b*-Cre (TPA) mice were treated with ECM remodeling inhibitors BAPN or LOX mAb followed by further analysis. (**B-D**) Shown are measurements on individual stiffness of multiple points in metastasized livers of TPA mouse model treated with IgG (**B**), LOX mAb (**C**) and BAPN (**D**). (**E**) IF staining displaying the expression and distribution of α-SMA and collagen I in liver metastatic niches of TPA mouse model (3 repeats performed per tissue, 3 fields assessed per sample). blue, DAPI; green, collagen I; red, α-SMA; scale bar, 25 μm. (**F-H**) CT FIRE analyzes the fibre data in liver metastasis of TPA mouse model including the fibre number (**G**) and variation (**H**) ($n=5$ mice per group, mean ± s.e.m.; two tailed unpaired t-test). (**I**) IF staining demonstrating the expression of TNNT1 in liver metastatic niches of differently treated TPA mouse model (3 repeats performed per tissue, 3 fields assessed per sample). blue, DAPI; green, collagen I; red, α-SMA; purple, TNNT1; scale bar, 25 μm. (**J**) Real-time PCR measuring the expression of *Tnnt1* in livers of differently treated TPA mouse models ($n=5$ mice per group, mean ± s.e.m.; two tailed unpaired t-test). (**K-L**) Intrasplenic injection mouse model evaluating the effect of ECM stiffness induced TNNT1 expression (3 repeats performed per tissue, 3 fields assessed per sample); blue, DAPI; purple, TNNT1; scale bar, 50 μm. (**M-O**) IF staining showing the relationship of TNNT1 and p27 expression using MFC cells expressing dormancy-awakening system (3 repeats performed per tissue, 3 fields assessed per sample); blue, DAPI; green, collagen I; red, α-SMA; scale bar, 25 μm

actively proliferating liver metastatic niches were usually surrounded by abundant ECM accompanied by complex TME influences. In contrast, smaller-diameter clones with negative proliferation indicators lacked ECM envelopment, and these dormant metastatic niches did not exhibit complex TME characteristics. This phenomenon suggests a significant association between ECM enrichment and dormancy-awakening processes of metastatic tumor cells. During the initial stages of metastatic tumor cell proliferation, the TME structure is relatively simple, highlighting the importance of ECM enrichment in its supportive role. Based on the analysis of clinical samples of GC liver metastasis regarding the size, proliferation, dormancy status of metastatic lesions, and the surrounding ECM, we hypothesized that ECM stiffness may play a crucial role in tumor cell awakening and proliferation within the liver during the process of metastasis. After the establishment of a highly reproducible dormancy-awakening detection system, we next performed an in vivo test to consolidate. We utilized an intrasplenic injection mouse model for study, since the injected murine cell line MFC would travel through portal vein before arriving at left lobe of liver, which effectively recapitulated the characteristics of tumor cells entering the liver through the portal vein to form metastatic niches at left lobe of liver [7, 27]. Additionally, CT combined 3D organ reconstruction bioluminescence imaging was performed to detect liver metastatic niches in mouse model. This approach effectively filtered background and false-positive signals, providing a direct visualization of metastatic niche sizes.

We also modeled two groups of mice by injecting MFC^{mCherry}/GFP-p27K^{-} alone and MFC^{mCherry}/GFP-p27K^{-}mixed with aHSCs respectively followed by assessing the dormancy status of tumor cells in metastatic niches and stiffness of ECM around them in both groups. In vivo experiments revealed a significant correlation between the dormancy/activation status of tumor cells in niches and the ECM stiffness. GFP^{+}/mCherry^{+} (dormant) and mCherry^{+} (activated) were then used for RNA-seq to filer out the key genes in response to ECM stiffness. Additionally, we also cultured tumor cells in vitro using gels of different stiffnesses (0.5 kPa and 40 kPa) for confirmation. Multiple in vivo and in vitro experiments not only demonstrated the correlation between ECM stiffness and tumor cell dormancy-activation status but also collectively screened out molecules significantly upregulated during the awakening process of dormant tumor cells caused by ECM stiffnesses, among which *TNNT1* were selected. We also use TPA mice, which could generate GC liver metastasis at 10-month-old spontaneously. In this model, the characteristics of liver metastasis is similar to those of GC patients, such as the enrichment of ECM with enhanced stiffness. As LOX have been demonstrated to have important roles in cross-linking collagen fibres, the LOX mAb or LOX inhibitor BAPN was performed to downregulate the stiffness of tumor niches. Especially, we have also reported that BAPN could hamper the reciprocal cross-talk of CAFs and tumor cells in GC liver metastasis [28], it is efficient to target dual mechanisms through BAPN administration. To consolidate, we used AFM to measure every individual point at one tissue and correlate which to TNNT1 expression using mIF. Our results have displayed that in area of higher and wider

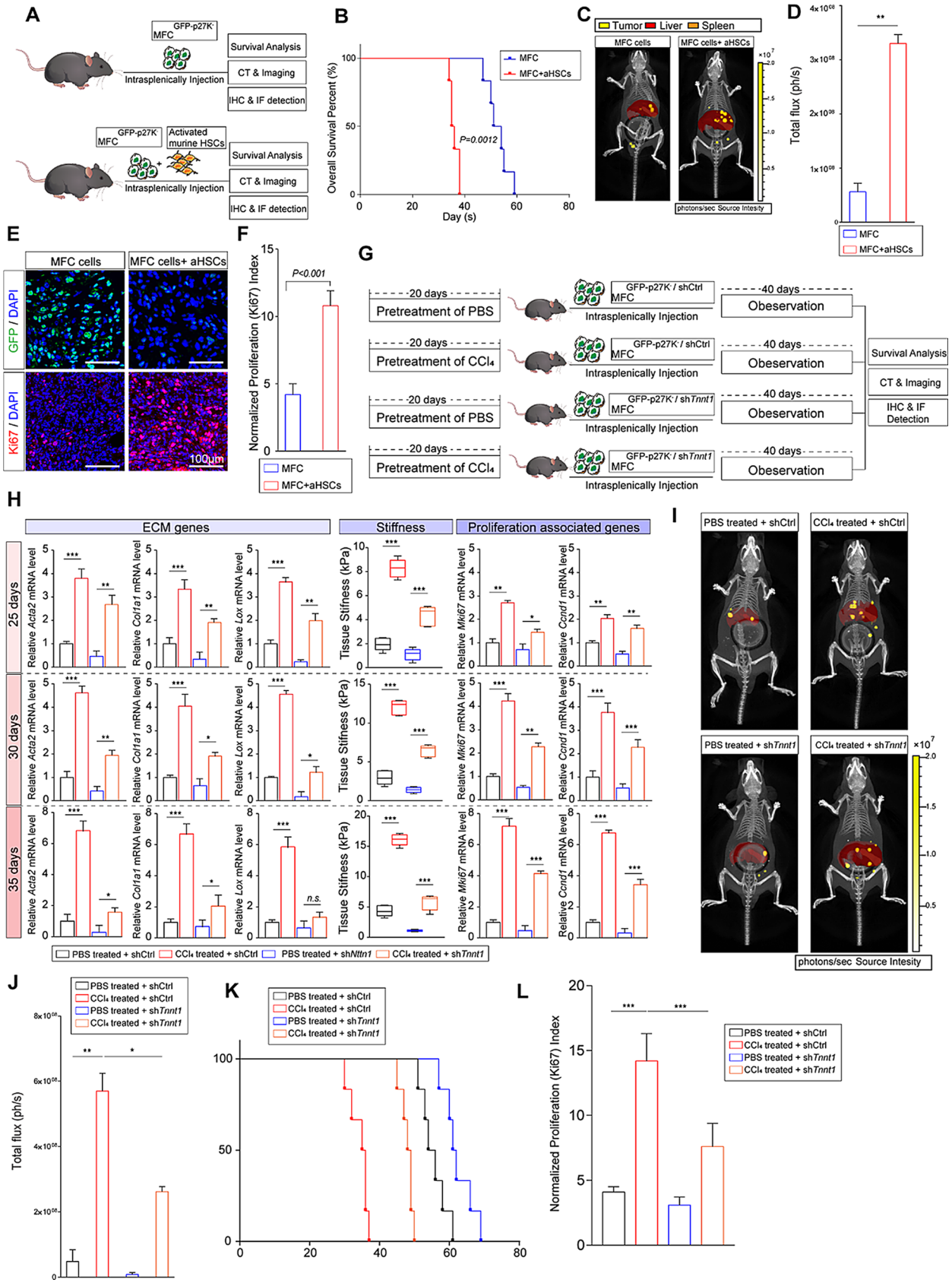
A
GFP-p27K- MFC
Intrasplenically Injection
Survival Analysis
CT & Imaging
IHC & IF detection
Activated murine HSCs
B
Overall Survival Percent (%)
Day (s)
MFC
MFC+aHSCs
P=0.0012
C
Tumor Liver Spleen
MFC cells
MFC cells+ aHSCs
photons/sec Source Intesity
D
Total flux (ph/s)
E
MFC cells
MFC cells+ aHSCs
GFP / DAPI
Ki67 / DAPI
100μm
F
Normalized Proliferation (Ki67) Index
P<0.001
G
20 days
Pretreatment of PBS
Pretreatment of CCl4
40 days
Obeservation
GFP-p27K- / shCtrl MFC
GFP-p27K- / shTnnt1 MFC
Survival Analysis
CT & Imaging
IHC & IF Detection
H
ECM genes
Stiffness
Proliferation associated genes
25 days
30 days
35 days
Relative Acta2 mRNA level
Relative Col1a1 mRNA level
Relative Lox mRNA level
Tissue Stifness (kPa)
Relative Mki67 mRNA level
Relative Ccnd1 mRNA level
n.s.
PBS treated + shCtrl
CCl4 treated + shCtrl
PBS treated + shNttn1
CCl4 treated + shTnnt1
I
PBS treated + shCtrl
CCl4 treated + shCtrl
PBS treated + shTnnt1
CCl4 treated + shTnnt1
photons/sec Source Intesity
J
Total flux (ph/s)
K
L
Normalized Proliferation (Ki67) Index

Fig. 6 TNNT1 overexpression facilitates activation of tumor cell. (**A**) Schematic illustration depicting the experimental strategy of intrasplenic injection of dormancy-awakening system-transfected MFC mixed with activated hepatic stellate cells. (**B**) Survival analysis illustrating differential survival prognosis of mice experienced intrasplenic injection of MFC tumor cells mixed with or without aHSCs ($n=5$ mice per group). (**C-D**) CT combined 3D organ reconstruction bioluminescence imaging assessing the progression of liver metastases in intrasplenic injection mouse models using MFC tumor cells mixed with or without aHSCs ($n=5$ mice per group, mean ± s.e.m.; two tailed unpaired t-test). Tumor signals, yellow; reconstructed liver, red; reconstructed spleen, orange. Scale color bar, 1.00×10^6-2.00×10^7. (**E-F**) IF staining displaying the distribution of dormant (GFP) and activated cells (Ki67) within mouse liver metastases; blue, DAPI; green, GFP; red, Ki67; scale bar, 100 μm. (**G**) Schematic diagram illustrating the experimental strategy of liver metastasis modeled by intrasplenic injection of dormancy-awakening system-transfected MFC with or without *Tnnt1* RNAi in PBS or carbon tetrachloride pre-treated mice. (**H**) Shown is expression levels of ECM genes (Left), Stiffness (Middle), and proliferation associated genes (Right) at different time points (25days, 30days or 35days) in liver metastatic livers of intrasplenic injection model mice ($n=5$ mice per group, mean ± s.e.m.; two tailed unpaired t-test). (**I-J**) CT combined 3D organ reconstruction bioluminescence imaging assessing the progression of liver metastases in intrasplenic injection mouse models using dormancy-awakening system-transfected MFC with or without *Tnnt1* RNAi in PBS or carbon tetrachloride pre-treated mice. ($n=5$ mice per group, mean ± s.e.m.; two tailed unpaired t-test). Tumor signals, yellow; reconstructed liver, red; reconstructed spleen, orange. Scale color bar, 1.00×10^6-2.00×10^7. (**K**) Analysis showing differences in survival outcomes of model mice ($n=6$ mice per group). (**L**) Shown is changes in proliferation index of tumor cells in liver metastatic niches via assessing the staining of Ki67

collagen fibres and lower co-efficiency of variation, more TNNT1 positive tumor cells could be observed.

According to previous studies, implantation of DTCs is a critical step in metastasis progress and the cross-talk between DTCs and tumor microenvironment is vital. In this study, we hypothesized that DTCs with TNNT1 expression performed advantages in survival and implantation at liver by enhanced extracellular matrix stiffness. It is demonstrated that *Tnnt1* expressed murine cell line MFC could be activated by aHSC, which facilitated the stiffness of liver metastatic niches (Fig. 6A and F). Furthermore, RNAi against *Tnnt1* significantly attenuated tumor burdens in carbon tetrachloride modeled mice, indicating that stiffness mediated dormancy-awakening of tumor cells required TNNT1 expression. Recent studies have reported the importance of premetastatic microenvironment and illustrated the activation of fibroblasts at metastatic niches was earlier than arrival of tumor cells in liver. Thus, we put forward that *Tnnt1* positive DTCs could be easier to implant at CAFs aggregated premetastatic microenvironment followed by outgrowth. Interestingly, our results also indicate that the knockdown of *Tnnt1* leads to downregulation of CAFs-associated ECM genes expression around the metastatic niches, including *Acta2* and *Collagen I*. There may be several reasons for this phenomenon. We used a chemically induced aHSCs model via injection of carbon tetrachloride, which fostered a pre-metastatic tumor microenvironment, while the ECM gene expressions induced by this model may not be as prominent as in real TME. It is illustrated that the expression of *Tnnt1* can promote tumor cell proliferation, thereby generating a positive feedback loop on ECM genes expression. Meanwhile TNNT1 protein is a cytoskeletal-associated protein, closely related to the mechanical stress sensing and migration behavior of tumor cells, and the knockdown of this gene may cause the tumor cells' response to stiffness sluggish, thereby reducing their survival capacity. This will further impair the ability of tumor cells to remodel the TME, leading to the downregulation of ECM gene expression.

Based on these experimental findings, we found that in GC liver metastasis, increased ECM stiffness could be observed in TME due to aberrant activation of CAFs and crosslinking of CAFs derived collagens, which thus awakens DTCs from dormancy, leading them to enter the cell cycle for proliferation. Then key regulator involved in this process is TNNT1. The expression and recruitment of TNNT1 protein enable tumor cells to sense external mechanical stress signals and rapidly proliferate for outgrowth (Fig. 7L). Although LOX is a crucial molecule for crosslinking collagen fibers, assessing tissue stiffness in clinical applications remains challenging. Therefore, TNNT1 is significant as it allows for the evaluation of tissue stiffness, enabling therapeutic interventions using LOX inhibitors or neutralizing antibodies. Further research and clinical validation of TNNT1's role in assessing and modulating tissue stiffness could refine

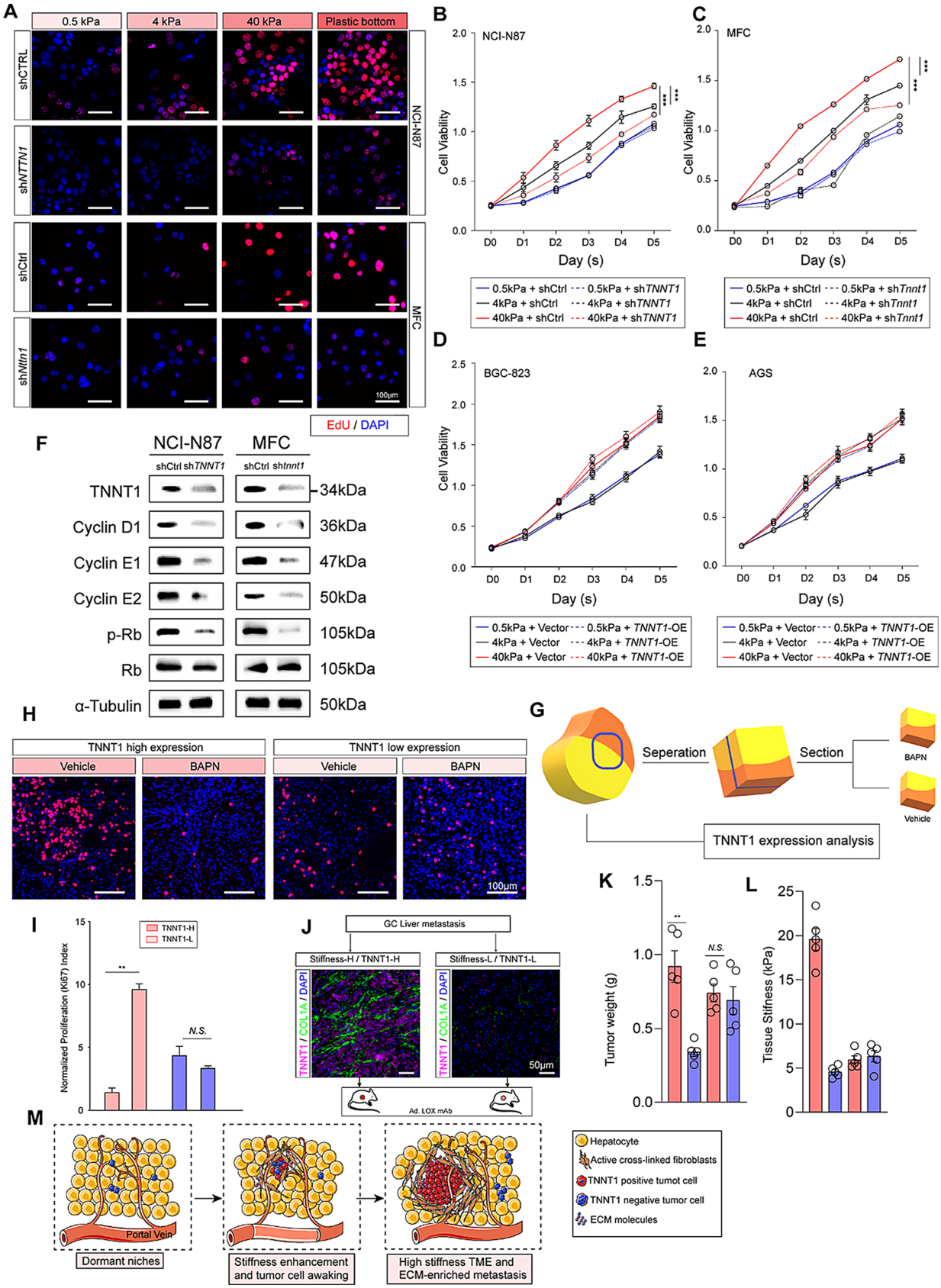
A
0.5 kPa
4 kPa
40 kPa
Plastic bottom
shCTRL
shNTTN1
shCtrl
shNtn1
NCI-N87
MFC
100μm
EdU / DAPI
B
NCI-N87
Cell Viability
Day (s)
0.5kPa + shCtrl
0.5kPa + shTNNT1
4kPa + shCtrl
4kPa + shTNNT1
40kPa + shCtrl
40kPa + shTNNT1
C
MFC
Cell Viability
Day (s)
0.5kPa + shCtrl
0.5kPa + shTnnt1
4kPa + shCtrl
4kPa + shTnnt1
40kPa + shCtrl
40kPa + shTnnt1
D
BGC-823
Cell Viability
Day (s)
0.5kPa + Vector
0.5kPa + TNNT1-OE
4kPa + Vector
4kPa + TNNT1-OE
40kPa + Vector
40kPa + TNNT1-OE
E
AGS
Cell Viability
Day (s)
0.5kPa + Vector
0.5kPa + TNNT1-OE
4kPa + Vector
4kPa + TNNT1-OE
40kPa + Vector
40kPa + TNNT1-OE
F
NCI-N87
MFC
shCtrl shTNNT1
shCtrl shtnnt1
TNNT1
Cyclin D1
Cyclin E1
Cyclin E2
p-Rb
Rb
α-Tubulin
34kDa
36kDa
47kDa
50kDa
105kDa
105kDa
50kDa
G
Seperation
Section
BAPN
Vehicle
TNNT1 expression analysis
H
TNNT1 high expression
TNNT1 low expression
Vehicle
BAPN
Vehicle
BAPN
100μm
I
TNNT1-H
TNNT1-L
Normalized Proliferation (Ki67) Index
**
N.S.
J
GC Liver metastasis
Stiffness-H / TNNT1-H
Stiffness-L / TNNT1-L
TNNT1 / COL1A / DAPI
50μm
Ad. LOX mAb
K
Tumor weight (g)
**
N.S.
L
Tissue Stiffness (kPa)
M
Portal Vein
Dormant niches
Stiffness enhancement and tumor cell awaking
High stiffness TME and ECM-enriched metastasis
Hepatocyte
Active cross-linked fibroblasts
TNNT1 positive tumot cell
TNNT1 negative tumor cell
ECM molecules

Fig. 7 TNNT1 provides potential therapeutic strategy for metastatic GC. (**A**) EdU staining on human GC liver metastatic cells line NCI-N87 and murine GC cell line MFC with or without TNNT1 (or Tnnt1) RNAi under different ECM stiffness (0.5 kPa, 4 kPa, 40 kPa or plastic bottom); blue, DAPI; red, Ki67; scale bar, 100 μm. (**B-C**) Cell viability measured by CCK-8 assay displaying the proliferation ability of NCI-N87 (**B**) or MFC (**C**) experienced RNAi of *TNNT1* or *Tnnt1* at different ECM stiffness (0.5 kPa,4 kPa and 40 kPa) ($n=5$ replicates per group, mean±s.e.m.; Repeat Measure ANOVA.) (**D-E**) Cell viability measured by CCK-8 assay showing BGC-823 (**D**) or AGS (**E**) cell line with overexpression of TNNT1 at different ECM stiffness (0.5 kPa,4 kPa and 40 kPa) ($n=5$ replicates per group, mean±s.e.m.; Repeat Measure ANOVA.). (**F**) Western Blott examining cell cycle pathway altered by RNAi of TNNT1 in NCI-N87 or MFC cell line. (**G-I**) Ex-vivo test measuring Ki67 staining on metastatic niches of different TNNT1 expression after BAPN administration (3 repeats performed per tissue, 3 fields assessed per sample); blue, DAPI; red, Ki67; scale bar, 100 μm. (**J-L**) Patients derived xenograft (PDX) mouse model evaluating the translational value of TNNT1 in GC liver metastasis(3 repeats performed per tissue, 3 fields assessed per sample, $n=5$ mice per group, mean±s.e.m.; two tailed unpaired t-test), blue, DAPI; green, collagen I, purple, TNNT1; scale bar, 50 μm. (**M**) Brief cartoon illustrating the backbone of discovery

diagnostic accuracy and therapeutic effectiveness in managing metastatic diseases effectively.

Supplementary Information The online version contains supplementary material available at https://doi.org/10.1007/s13402-025-01053-w.

Acknowledgements We thank Dr Gang Zhao for his kind assistances.

Author contributions Z.Z.Z., C.C.Z. and B.N. were responsible for concept and experimental design; L.H.J., Z.Z.Z. and C.C.Z. were responsible for clinical samples collection; L.H.J., J.P., Y.X.L. and Y.Q.Z. were responsible for experiments, L.H.J. and J.P. wrote the main manuscript text and L.H.J., J.P. and Y.X.L. prepared figures.

Funding This study is supported by National Natural Science Foundation of China (82173215, 82473077) by Zizhen Zhang; National Natural Science Foundation of China (82303428) by Bo Ni.

Data availability No datasets were generated or analysed during the current study.

Declarations

Ethical approval The collection of clinical samples from gastric cancer patients at Renji Hospital was approved by the Ethics Committee of Renji Hospital (Approval No. RA-2019-116.1), with informed consent obtained from all participants. The animal experiments were approved by the Research Ethics Committee of East China Normal University (Approval No. 20141204) and conducted in accordance with the Guide for the Care and Use of Laboratory Animals.

Competing interests The authors declare no competing interests.

References

1. H. Sung et al., Global Cancer statistics 2020: GLOBOCAN estimates of incidence and mortality worldwide for 36 cancers in 185 countries. CA Cancer J. Clin. **71**(3), 209–249 (2021)
2. L.P. Carcas, Gastric cancer Rev. J. Carcinog. **13**, 14 (2014)
3. A. Cervantes et al., Current questions for the treatment of advanced gastric cancer. Cancer Treat. Rev. **39**(1), 60–67 (2013)
4. K. Shitara et al., Reporting patient characteristics and stratification factors in randomized trials of systemic chemotherapy for advanced gastric cancer. Gastric Cancer. **15**(2), 137–143 (2012)
5. S. Paget, The distribution of secondary growths in cancer of the breast. 1889. Cancer Metastasis Rev. **8**(2), 98–101 (1989)
6. Y. Liu, X.T. Cao, Characteristics and significance of the Pre-metastatic niche. Cancer Cell. **30**(5), 668–681 (2016)
7. S.R. Nielsen et al., Macrophage-secreted granulin supports pancreatic cancer metastasis by inducing liver fibrosis. Nat. Cell. Biol. **18**(5), 549–560 (2016)
8. J. Albrengues et al., Neutrophil extracellular traps produced during inflammation awaken dormant cancer cells in mice. Science. **361**(6409), (2018)
9. C.M. Ghajar, Metastasis prevention by targeting the dormant niche. Nat. Rev. Cancer. **15**(4), 238–247 (2015)
10. A. Pommier et al., Unresolved Endoplasmic reticulum stress engenders immune-resistant, latent pancreatic cancer metastases. Science. **360**(6394), (2018)
11. Q. Li et al., Coadaptation fostered by the SLIT2-ROBO1 axis facilitates liver metastasis of pancreatic ductal adenocarcinoma. Nat. Commun. **14**(1), 861 (2023)
12. T. Oki et al., A novel cell-cycle-indicator, mVenus-p27K-, identifies quiescent cells and visualizes G0-G1 transition. Sci. Rep. **4**, 4012 (2014)
13. J. Vlach, S. Hennecke, B. Amati, Phosphorylation-dependent degradation of the cyclin-dependent kinase inhibitor p27. EMBO J. **16**(17), 5334–5344 (1997)
14. Y. Dong et al., Higher matrix stiffness as an independent initiator triggers epithelial-mesenchymal transition and facilitates HCC metastasis. J. Hematol. Oncol. **12**(1), 112 (2019)
15. H. He et al., Higher matrix stiffness promotes VSMC senescence by affecting mitochondria-ER contact sites and mitochondria/er dysfunction. FASEB J. **37**(12), e23318 (2023)
16. A. Nicolas-Boluda et al., Tumor stiffening reversion through collagen crosslinking Inhibition improves T cell migration and anti-PD-1 treatment. Elife. **10** (2021)
17. K.R. Levental et al., Matrix crosslinking forces tumor progression by enhancing integrin signaling. Cell. **139**(5), 891–906 (2009)
18. S. Seton-Rogers, Fibroblasts shape PDAC architecture. Nat. Rev. Cancer. **19**(8), 418 (2019)
19. O. Maller et al., Tumour-associated macrophages drive stromal cell-dependent collagen crosslinking and stiffening to promote breast cancer aggression. Nat. Mater. **20**(4), 548–559 (2021)
20. Y. Chen et al., Lysyl hydroxylase 2 induces a collagen cross-link switch in tumor stroma. J. Clin. Invest. **125**(3), 1147–1162 (2015)

21. M.C. Lampi, C.A. Reinhart-King, Targeting extracellular matrix stiffness to attenuate disease: from molecular mechanisms to clinical trials. Sci. Transl Med. **10**(422), (2018)
22. S. Zhang et al., Transglutaminases are oncogenic biomarkers in human cancers and therapeutic targeting of TGM2 blocks chemoresistance and macrophage infiltration in pancreatic cancer. Cell. Oncol. (Dordr). **46**(5), 1473–1492 (2023)
23. Y. Shi et al., TNNT1 facilitates proliferation of breast cancer cells by promoting G(1)/S phase transition. Life Sci. **208**, 161–166 (2018)
24. J. Wang et al., Cuproptosis-related risk score predicts prognosis and characterizes the tumor microenvironment in colon adenocarcinoma. Front. Oncol. **13**, 1152681 (2023)
25. X. Xia et al., Neutrophil extracellular traps promote metastasis in gastric cancer patients with postoperative abdominal infectious complications. Nat. Commun. **13**(1), 1017 (2022)
26. T. Higashi, S.L. Friedman, Y. Hoshida, Hepatic stellate cells as key target in liver fibrosis. Adv. Drug Deliv. Rev. **121**, 27–42 (2017)
27. B. Ni et al., Tumor-associated macrophage-derived GDNF promotes gastric cancer liver metastasis via a GFRA1-modulated autophagy flux. Cell. Oncol. (Dordr). **46**(2), 315–330 (2023)
28. Q. Li et al., Lysyl oxidase promotes liver metastasis of gastric cancer via facilitating the reciprocal interactions between tumor cells and cancer associated fibroblasts. EBioMedicine. **49**, 157–171 (2019)